IV International Conference on Particle-based Methods – Fundamentals and Applications
PARTICLES 2015
E. Oñate, M. Bischoff, D.R.J. Owen, P. Wriggers & T. Zohdi (Eds)

# TIME-DEPENDENT DEM BASED FRACTURE SIMULATIONS AT THE GRAIN SIZE LEVEL FOR BRITTLE HETEROGENEOUS SOLIDS

**HEINZ KONIETZKY[1], WEI CHEN[2]**

[1] Chair for Rock Mechanics, Geotechnical Institute, TU Bergakademie Freiberg, Germany
09599 Freiberg, Germany
e-mail: Heinz.Konietzky@ifgt.tu-freiberg.de
web page: http://tu-freiberg.de/fakult3/gt/feme/mitarb/konietz.en.html

[2] Chair for Rock Mechanics, Geotechnical Institute, TU Bergakademie Freiberg, Germany
09599 Freiberg, Germany
e-mail: chenwei.csu@foxmail.com
web page: http://tu-freiberg.de/fakult3/gt/feme/mitarb/chen.html

**Key words:** Discrete Element Method, Heterogeneous Granite, Time-dependent Fracture.

**Abstract.** A discrete element numerical model for Lac du Bonnet granite is built for time-dependent fracture simulations. The heterogeneity is considered by different mineral components randomly distributed inside the rock. The minerals are represented by elastic Voronoi cells connected by elasto-plastic contacts. The Hillig-Charles equation is implanted in the numerical model for analyzing time-dependent damage due to subcritical crack growth. The damage processes during uniaxial compressive creep tests are investigated. The numerical simulations reveal not only reasonable lifetime of the specimens under different loads, but also show primary, secondary and tertiary creep stages until final failure characterized by macroscopic fracturing. The simulation results of crack growth and damage index evolution deliver a deeper insight into the microscopic damage process.

## 1 INTRODUCTION

Time-dependent damage of rocks is especially important for long-term stability and safety of geotechnical structures such as mines, tunnels, and nuclear waste repositories. The time-dependent damage in brittle rocks has a close relationship to subcritical crack growth. Analysis of time-dependent damage of brittle rocks has been carried out by many scientists using both, continuum and discrete element based methods.

For a continuum based method: According to theory of subcritical crack growth, Konietzky et al. [1] proposed a numerical model to simulate the lifetime of rocks under static loads by growing microcracks. Li and Konietzky [2,3,4] developed this approach further by taking into account stochastic distributions for initial length and orientation of microcracks and different crack growth models.

For discrete element method: Kemeny [5] developed a fracture mechanical model, considering the degradation of cohesive strength of rocks due to subcritical crack growth, to simulate time-dependent failure of rock bridges along discontinuities. Lee [6] analyzed the time-dependent stability of Coconino rock slope using UDEC based on the method proposed

by Kemeny [5]. Park [7] introduced a numerical method in PFC to investigate time-dependent fracture growth in rocks. Potyondy [8] used PFC to simulate static fatigue of granite due to stress corrosion.

In this paper, the explicit consideration of time-dependent damage evolution due to subcritical crack growth until final failure is analyzed. UDEC is adopted to perform the numerical simulations utilizing the embedded constitutive laws for elastic grains and elasto-plastic contacts, but extended by incorporating own developed routines to simulate subcritical crack growth.

## 2 THEORY OF SUBCRITICAL CRACK GORWTH

The relationship between subcritical crack growth velocity and stress intensity factor is illustrated in Figure 1. As discussed by many researchers [8,9,10,11], $K_{I0}$ is the lower limit stress intensity factor, below which the crack is stable. $K_{Ic}$ is the Mode I fracture toughness at the time when the velocity of crack growth suddenly approaches critical values and causes failure. In region 1 (Figure 1), the velocity is controlled by the rate of stress corrosion reactions at the crack tips. In region 2, the velocity is controlled by the rate of transport of reactive species to the crack tips and in region 3, crack growth is mainly ruled by mechanical rupture and is relatively insensitive to the environment.

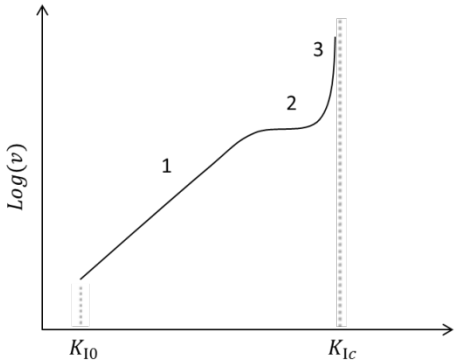


**Figure 1**: Crack growth velocity versus stress intensity factor [10]

Hillig-Charles equation (exponential law) is frequently used to describe the subcritical crack growth (region 1 of Figure 1). Hillig and Charles [12] made the hypothesis that the static fatigue in glass follows the rule of chemical reaction between the glass and the environment, but they have also recognized that the process is stress-sensitive. According to their findings, they proposed a quantitative equation for describing crack velocity:

$$v = v_0 \exp\left[\left(-E + V\sigma - V_m\gamma/\rho\right)/RT\right] \tag{1}$$

where $E$ is the stress free activation energy, $V$ is the activation volume, $\sigma$ is the tensile stress at the crack tip, $V_m$ is the molar volume of the material, $\gamma$ is the interfacial surface energy between the glass and the reaction products, $\rho$ is the radius of the curvature of the crack tip, $R$ is the gas constant and $T$ is the absolute temperature.

Wiederhorn and Bolz [13] have re-written Eq. (1) by introducing the two-dimensional Griffith crack term $\sigma = 2K_I/\sqrt{\pi\rho}$:

$$\begin{cases} v = v_0 \exp\left[\left(-E_* + 2VK_I/\sqrt{\pi\rho}\right)/RT\right] \\ E_* = E + V_m\gamma/\rho \end{cases} \tag{2}$$

Based on Eq. (2), Wiederhorn et al. [14] have proposed an empirical relation by fitting lab test data from glass with least square method:

$$v = v_0 \exp\left[\left(-E_* + bK_I\right)/RT\right] \tag{3}$$

where $b$ is empirical constant obtained from the fitting curve.

Eq. (3) was successfully used to analyze subcritical crack growth in rocks [8,10,15].

## 3 NUMERICAL MODEL

### 3.1 Grain-based heterogeneous model

The mineral composition of Lac du Bonnet (LdB) granite is characterized by 7.1% biotite, 51.1% K-feldspar, 31.8% quartz and 10% plagioclase. The smallest grains have a diameter of about 1 mm. They are randomly distributed within a piece of rock. The numerical model was created by Voronoi cells with equivalent diameter of about 1 mm. The percentages of the mineral components were considered and the allocation was performed in a random manner, so that the model matches the grain size distribution in an approximate manner and also bigger grain clumps (mineral clumps) were automatically produced (Figure. 2). The Voronoi cells itself are unbreakable and behave elastically. The height and the diameter of numerical model are 63.4mm and 31.7mm, respectively. The parameters for the mineral components and Voronoi cells, respectively, are given in Table 1.

**Table 1**: Grain parameters [16,17,18]

| Mineral | Elastic Modulus (GPa) | Poisson's Ratio |
|---|---|---|
| Biotite | 35 | 0.25 |
| K-feldspar | 62 | 0.27 |
| Quartz | 91 | 0.20 |
| Plagioclase | 69 | 0.23 |

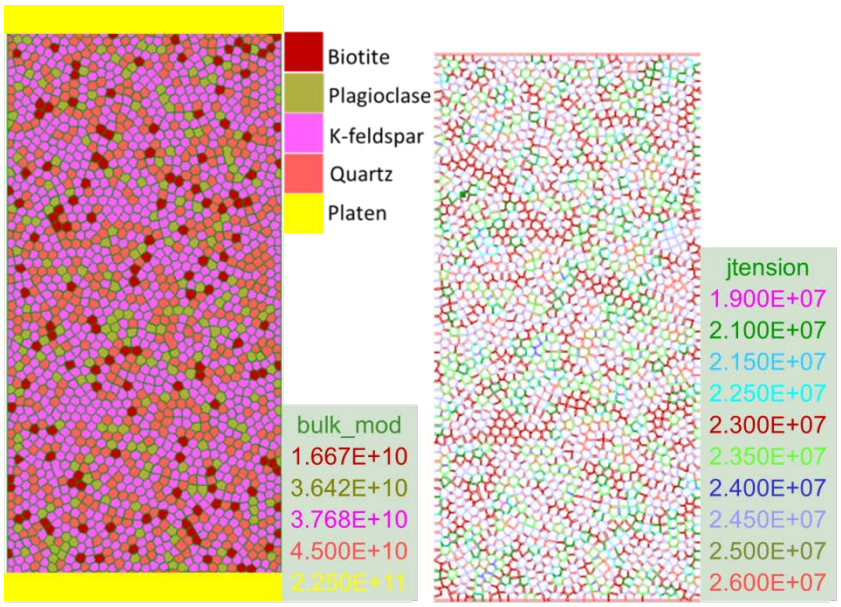


(a) (b)

**Figure 2**: Model set-up: (a) Voronoi blocks representing different minerals, (b) contacts between minerals

The contact behavior is elasto-plastic and characterized by a Mohr-Coulomb failure criterion with tension cut-off and softening (Figure. 3). For each mineral component, a corresponding set of contact parameters is specified (Table 2). At the contacts between the grains, the arithmetic average of the parameters is applied. Parameters shown in Table 2 are obtained by numerical back-analysis of time-independent loading tests. The simulated and experimental uniaxial compressive strength is 234.5 MPa and 200±22 (n=81) MPa [19], respectively. In the normal and shear direction, the stress-displacement relation below the strength limit at the contacts is assumed to be linear and governed by the normal stiffness $k_n$ and the shear stiffness $k_s$. If the tensile strength is reached, the contact breaks and the tensile strength is set to zero. If the shear strength is reached, sudden softening takes place and cohesion and friction of the contact are set to residual values. Eqs. (4) and (5) describe the contact behavior:

$$\begin{cases} \sigma_n = -k_n u_n \\ if\ \sigma_n < -J^T,\ \sigma_n = J_r^T = 0 \end{cases} \tag{4}$$

$$\begin{cases} \tau_s = k_s u_s \\ \tau_{\max} = J^C + \sigma_n \tan\varphi \\ if\ |\tau_s| \geq \tau_{\max},\ \tau_s = sign(\Delta u_s) \cdot \left(J_r^C + \sigma_n \tan\varphi_r\right) \end{cases} \tag{5}$$

where $\sigma_n$ and $\tau_s$ are normal stress and shear stress, respectively, $u_n$ and $u_s$ are normal displacement and shear displacement, respectively, $J^T$ and $J_r^T$ are tensile strength and residual

tensile strength, respectively, $\tau_{\max}$ is shear strength, $J^C$ and $J_r^C$ are cohesive strength and residual cohesive strength , respectively, $\varphi$ and $\varphi_r$ are friction angle and residual friction angle, respectively, and $\Delta u_s$ is the incremental contact shear displacement.

Within the model the damage and fracture process associated with plastic deformations is controlled by the breakage of contacts and relative movement along or across them.

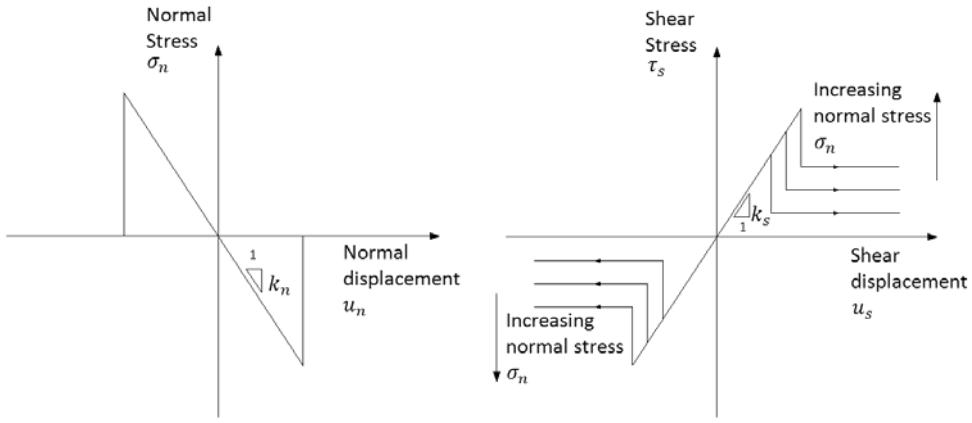


(a) (b)

**Figure 3**: Elasto-plastic contact behaviour with softening: (a) in normal direction, (b) in shear direction

**Table 2**: Contact parameters (result of own calibration)

| Contact | $k_n$ (Pa/m) | $\frac{k_s}{k_n}$ | $J^T$ (MPa) | $J_r^T$ (MPa) | $J^C$ (MPa) | $J_r^C$ (MPa) | $\varphi$ (°) | $\frac{\varphi_r}{\varphi}$ |
|---|---|---|---|---|---|---|---|---|
| Biotite/Biotite | 4.20E+14 | 1 | 19 | 0 | 37 | 0 | 48 | 0.5 |
| K-feldspar/K-feldspar | 7.75E+14 | 1 | 23 | 0 | 52 | 0 | 55 | 0.5 |
| Quartz/Quartz | 1.01E+15 | 1 | 26 | 0 | 62 | 0 | 62 | 0.5 |
| Plagioclase/Plagioclase | 8.00E+14 | 1 | 24 | 0 | 57 | 0 | 59 | 0.5 |
| Biotite/K-feldspar | 5.97E+14 | 1 | 21 | 0 | 44.5 | 0 | 51.5 | 0.5 |
| Biotite/Quartz | 7.16E+14 | 1 | 22.5 | 0 | 49.5 | 0 | 55 | 0.5 |
| Biotite/Plagioclase | 6.10E+14 | 1 | 21.5 | 0 | 47 | 0 | 53.5 | 0.5 |
| K-feldspar/Quartz | 8.93E+14 | 1 | 24.5 | 0 | 57 | 0 | 58.5 | 0.5 |
| K-feldspar/Plagioclase | 7.87E+14 | 1 | 23.5 | 0 | 54.5 | 0 | 57 | 0.5 |
| Quartz/Plagioclase | 9.06E+14 | 1 | 25 | 0 | 59.5 | 0 | 60.5 | 0.5 |

### 3.2 Implementation Hillig-Charles equation into the numerical model

In order to consider subcritical crack growth, Hillig-Charles equation was implemented into UDEC under the assumption, that stress corrosion only affects contacts and not the rock matrix. Therefore, subcritical cracks can only propagate along the edges of the Voronoi cells. This leads to a time-dependent reduction of tensile and cohesive strength at the corresponding contacts. The degradation rates at the contacts are stress-dependent. The degradation for tensile strength

and cohesive strength of the contact is only influenced by tensile and shear stress in the contact.

Taking into account the above-mentioned assumptions and Eq. (1), the degradation rates can be described as follows:

$$\begin{cases} \dfrac{dJ_i^T}{dt} = -\lambda_r v_t = -\left(\lambda_r v_0 e^{-(E+V_m\gamma/\rho)/RT}\right) e^{V\overline{\sigma}_i/RT} \\ \dfrac{dJ_i^C}{dt} = -\lambda_r v_c = -\left(\lambda_r v_0 e^{-(E+V_m\gamma/\rho)/RT}\right) e^{V\overline{\tau}_i/RT} \end{cases} \tag{6}$$

where $J_i^T$ and $J_i^C$ are tensile and cohesive strengths at the contact $i$, respectively, $\lambda_r$ is a constant describing the proportionality between strength degradation and subcritical crack growth velocity, $v_t$ and $v_c$ are crack growth velocities governed by the level of tensile and shear stress at the contact, respectively, $\overline{\sigma}_i = F_i^n / L_i$ and $\overline{\tau}_i = F_i^s / L_i$ are average tensile and shear stresses at the contact, respectively, $F_i^n$ and $F_i^s$ are normal and shear forces at the contact, respectively, and $L_i$ is the contact length.

Assuming that $\beta_1 = \lambda_r v_0 e^{-(E+V_m\gamma/\rho)/RT}$ and $\beta_2 = V/RT$, and considering the constitutive model of the contacts, Equation (6) can be re-written into the following simple form:

$$\begin{cases} \dfrac{dJ_i^T}{dt} = \begin{cases} -\beta_1 e^{\beta_2\overline{\sigma}_i}, & \overline{\sigma}_i < J_i^T \\ -\infty, & \overline{\sigma}_i \geq J_i^T \end{cases} \\ \dfrac{dJ_i^C}{dt} = \begin{cases} -\beta_1 e^{\beta_2\overline{\tau}_i}, & \overline{\tau}_i < \tau_{\max(i)} \\ -\infty, & \tau_i \geq \tau_{\max(i)} \end{cases} \end{cases} \tag{7}$$

where $\tau_{\max(i)}$ is the shear strength at the contact $i$.

The contact strength decreases with time elapsing are ruled by Eq. (7). After a certain period of time, the contact strength degrading velocity approaches infinite, meaning that sudden failure at the contact occurs. The stresses around this failed contact will be redistributed and may cause further local stress concentrations, so that strength degrading at neighboring contacts will accelerate.

## 4 TIME-DEPEDENT DAMAGE SIMULATIONS

### 4.1 Uniaxial compressive creep test simulations

Schmidtke and Lajtai [20] have used 126 specimens of LdB granite to perform uniaxial compressive creep tests. The cylindrical specimen with a diameter of 37.1 mm was saturated before testing and kept submerged during testing at a temperature of 25°C. The numerical modelling approach implemented in Eq. (7) was used to simulate uniaxial compressive creep tests. The subcritical crack growth parameters are $\beta_1 = 0.001$ Pa/s and $\beta_2 = 1.0\times10^{-7}$. The other parameters are taken from Tables 1 and 2.

To minimize CPU time and to guarantee that the damage process is followed with sufficient precision, a changeable time step scheme is used for the simulations:

$$\begin{cases} \Delta t_{\min} \le \Delta t_b \le \Delta t_{\max} \\ if\ F_u < 100N, \Delta t_b = 2 * \Delta t_{b-1} \\ if\ F_u \ge 100N, \Delta t_b = \Delta t_{\min} \end{cases} \quad (8)$$

where $\Delta t_{\min}$, $\Delta t_b$ and $\Delta t_{\max}$ are the minimum, actual and maximum time steps respectively, and $F_u$ is the unbalance force, $b$ is the corresponding step number. For one-edged crack growth simulations we specified $\Delta t_{\min} = 1.0 \times 10^{-5}$ s and $\Delta t_{\max} = 1.0 \times 10^{4}$ s.

Results from lab tests [20] and numerical simulations with respect to lifetime (time to failure) for LdB granite under different driving-stress ratios are shown in Figure 4. The driving-stress ratio is defined by $\sigma/\sigma_c$ ($\sigma$ and $\sigma_c$ are uniaxial actual compressive stress and uniaxial compressive strength, respectively). The data show, that lifetime of specimens decrease with increasing driving-stress ratio. For different specimens under the same driving-stress ratio, there are variations in lifetime due to the heterogeneity of rock samples.

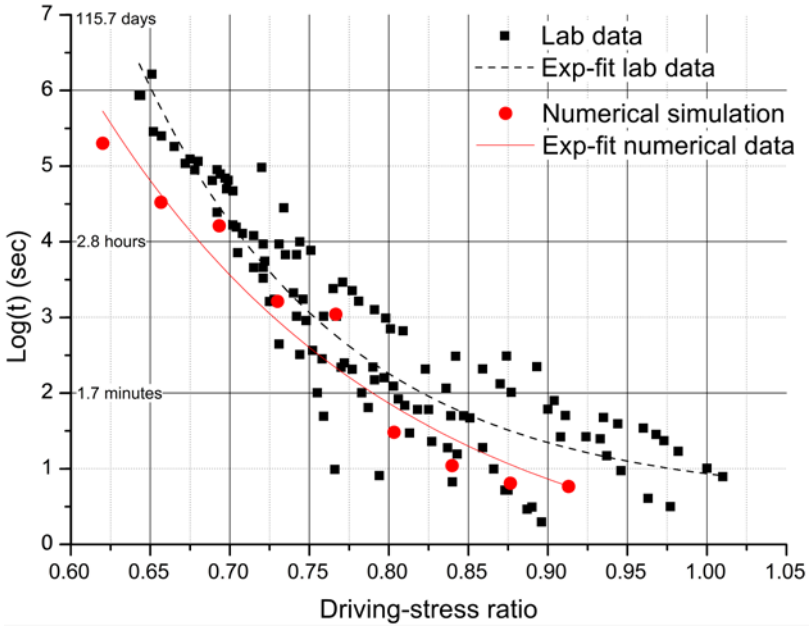


**Figure 4**: Lab test [20] and numerical simulation results for lifetime of LdB granite under different driving-stress ratios

Figure 5 shows simulation results of uniaxial compressive creep tests, which reveal primary, secondary and tertiary creep phases. The curves in Figure 5b is smoother than those in Figure 5a, because time steps change automatically in one case (Figure 5a) and are constant, that means equal to $\Delta t_{\min}$, in the other case (Figure 5b). The introduction of changeable time steps is necessary whenever huge lifetime is expected, which is the case for low load levels. Lifetime increases in a strong non-linear manner with decreasing load.

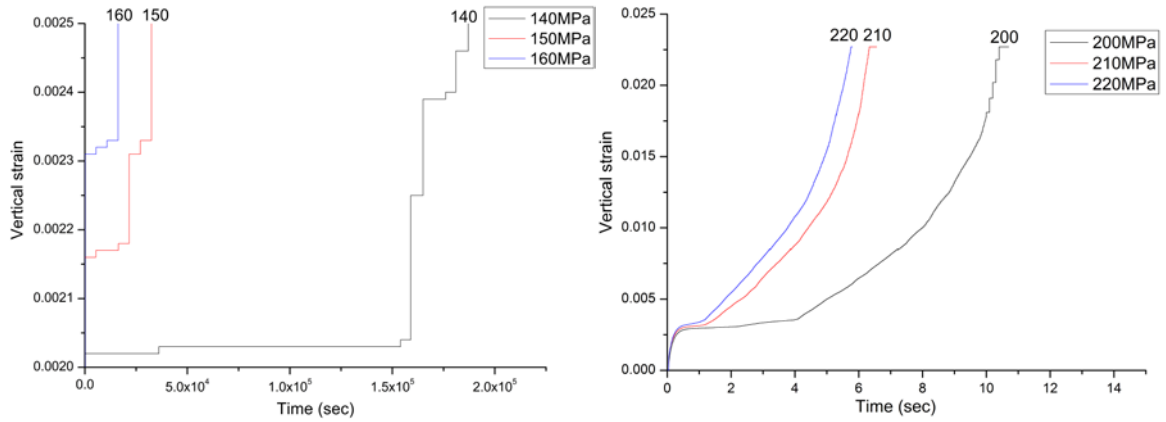


(a) (b)

**Figure 5**: Uniaxial creep simulation results for strain versus time: (a) load range 140-160 MPa, (b) load range 200-220 MPa

Figure 6 shows how contact failure (microcracks) and strain develop with ongoing time under constant load of 160 MPa. The rate of contact bond breakage (microcrack development) shows some correlation to the creep phases: the rate is relatively low within the secondary creep phase, but shows stronger values at the primary and tertiary creep phases.

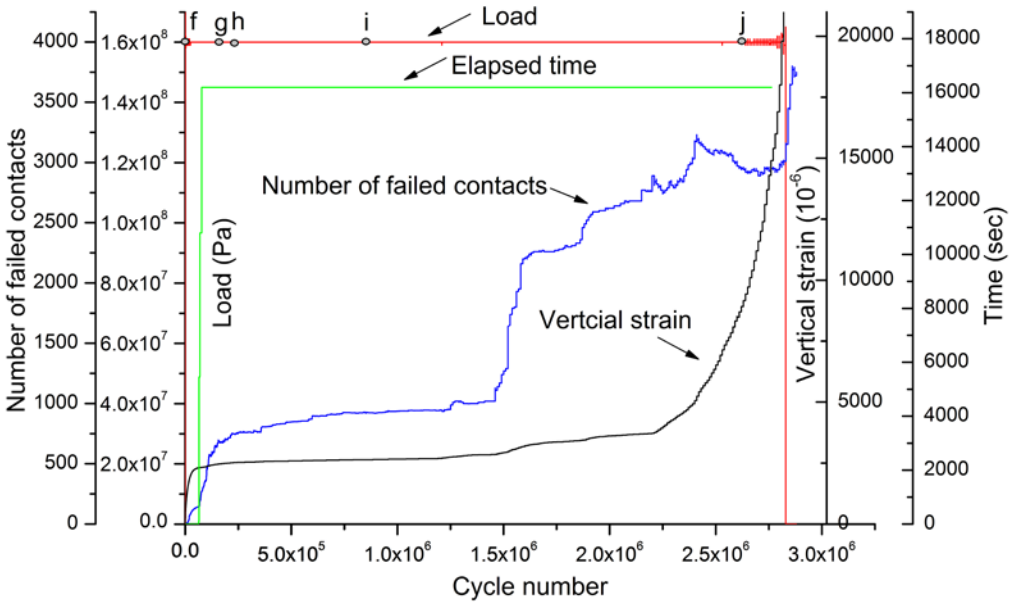


**Figure 6**: Simulation results of uniaxial creep tests under 160 MPa

Exemplary, macrocrack (totally detached contacts) distribution inside the specimen for a load level of 160 MPa for different points in time according to Figure 6 is shown in Figure 7. During the primary phase cracks emerge in a more random manner within the specimen (Figure 7g). Later, within the secondary creep phase, cracks grow further, interact with each other and form larger cracks mainly parallel to the maximum stress direction (Figure 7h-j). Finally, within the tertiary creep phase, massive crack interactions are observed and, in addition to large

vertical cracks, shear band formation is observed until final macroscopic failure is noticed (Figure 7 j).

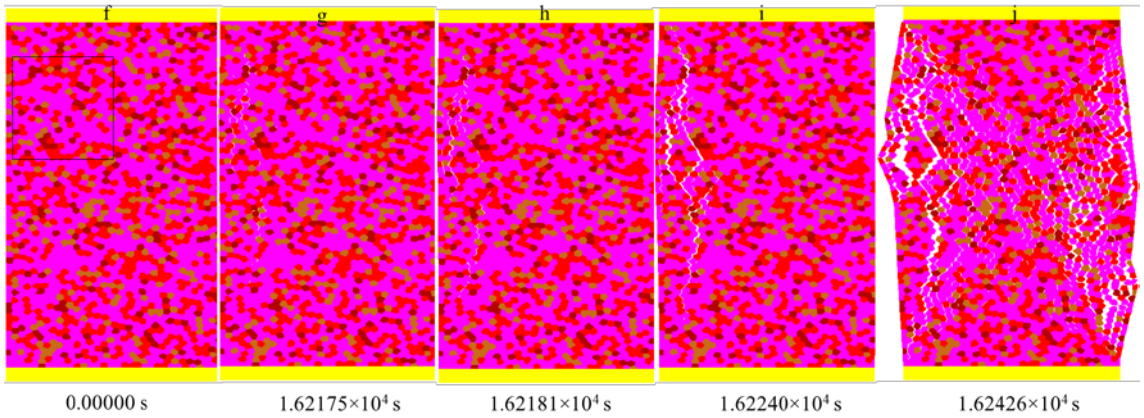


**Figure 7**: Macrocracks distribution under 160 MPa uniaxial compressive load for different points in time according to Figure 6

## 4.2 Crack growth and damage characteristic

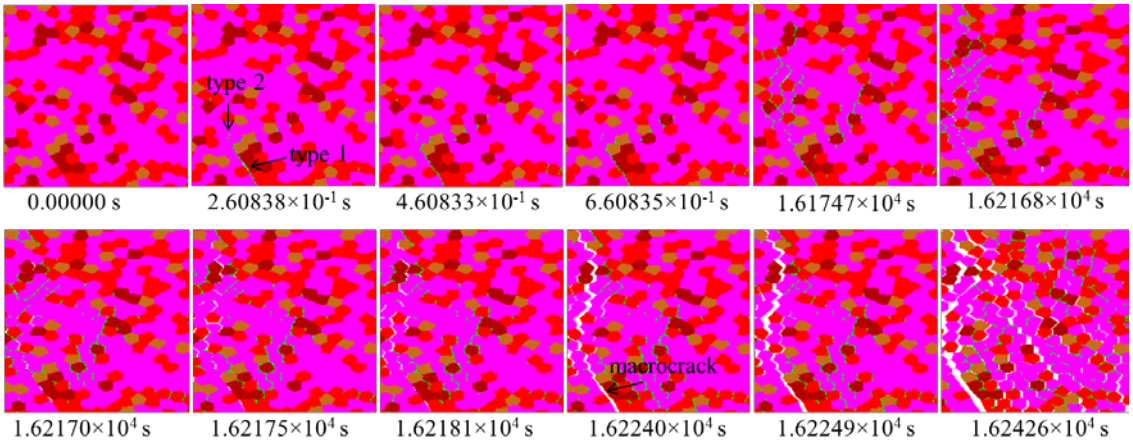


**Figure 8**: Microcrack and macrocrack distribution with time elapsing in a magnified viewing area indicated by black quadrangle in Figure 7f

Microcrack and macrocrack distribution with time elapsing in a magnified viewing area indicated by black quadrangle in Figure 7f is shown in Figure 8. The green lines and white space represent microcracks (position of failed contacts) and macrocracks (totally detached contacts which are the result of progressive crack development), respectively. At first the microcracks are randomly distributed within the specimen, but preferred occurring at the contacts between different minerals (type 1: inter-granular microcrack at $2.60838\times10^{-1}$ s) and with less preference in the contacts between the same minerals (type 2: intra-granular microcrack at $2.60838\times10^{-1}$ s). With time elapsing, more and more microcracks emerge, coalesce and form networks. Finally, this leads to occurrence of macrocracks, which is

illustrated by type 1 microcrack at $2.60838\times10^{-1}$ s, and which develops further towards a totally opened macrocrack at $1.62240\times10^{4}$ s. As shown in Figure 8a, initially, the propagation of subcritical crack due to stress corrosion is very time consuming (from 0 s to $1.62170\times10^{4}$ s). But once the microcrack network has formed (that means stress concentration phenomenon is serious), the speed of subcritical crack growth increases suddenly, and soon the macrocrack network is created and cause failure of the specimen (from $1.62170\times10^{4}$ s to $1.62426\times10^{4}$ s).

The damage index evaluated by number of failed contacts is defined as:

$$D_n = \frac{N_{ct}}{N_{c\max t}} \tag{9}$$

where $N_{ct}$ is the instantaneous number of failed contacts at elapsed time $t$ and $N_{c\max t}$ is the maximum number of failed contacts at $t_f$ (time to failure).

Simulation results in terms of damage index evolution versus normalized time elapsing is shown in Figure 9. The damage index evolution under high and low loadings is different. For the specimen under 160 MPa load, the damage index increases slowly with time elapsing during secondary creep stage (very time consuming) and then accelerates suddenly causing failure of specimen with typical tertiary creep phenomena. But for the specimen under 200 MPa load, the damage index develops quickly from beginning until failure occurs.

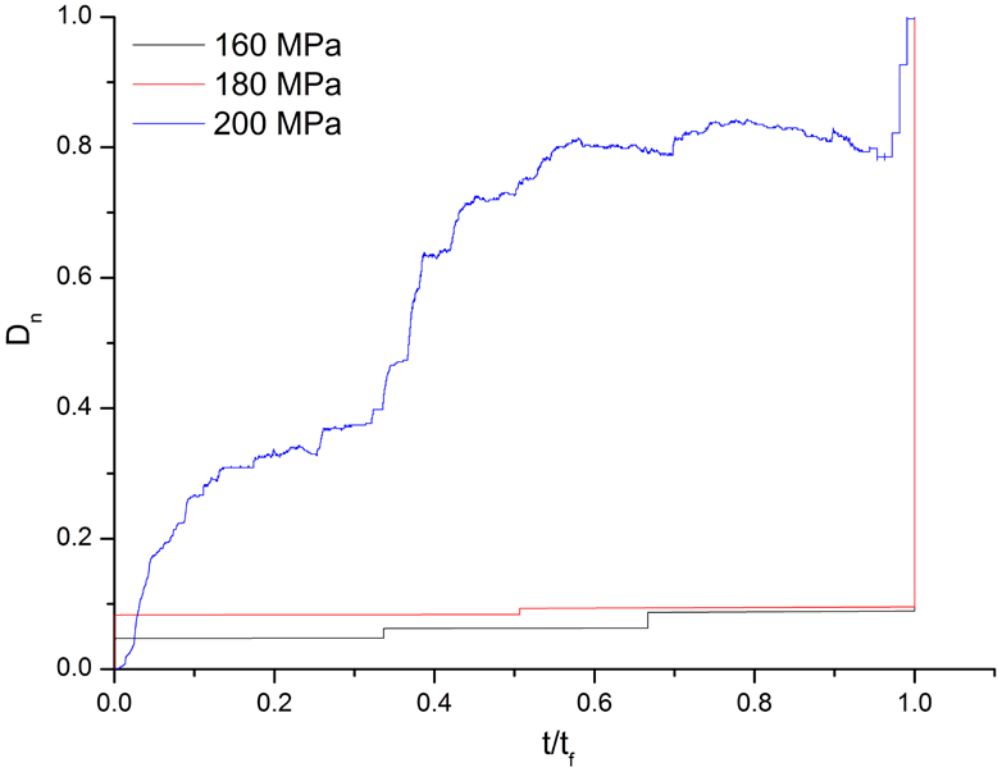


**Figure 9**: Damage index evaluated by number of failed contacts

## 5 CONCLUSIONS

- A modeling approach is presented, where the heterogeneity of the rock is realized by explicit considering the mineral components with different block and contact parameters.
- Uniaxial compressive creep of the rock has been analyzed by this numerical approach which has incorporated the Hillig-Charles equation for taking into account subcritical crack growth.
- The time-dependent fracture and damage evolution of rock samples under uniaxial compressive load has been studied at the grain size level in detail by the proposed numerical approach and shown satisfying agreement in terms of fracture pattern and time-dependent failure.

## REFERENCES

[1] Konietzky, H. Heftenberger, A. and Feige, M. Life time prediction for rocks under static compressive and tensile loads - a new simulation approach. Acta Geotechnica (2009) 4, 73-78.
[2] Li, X. and Konietzky, H. Time to Failure Prediction Scheme for Rocks. Rock Mech Rock Eng (2014) 47,1493-1503.
[3] Li, X. and Konietzky, H. Simulation of time-dependent crack growth in brittle rocks under constant loading conditions. Engineering Fracture Mechanics (2014) 119, 53-65.
[4] Li, X. and Konietzky, H. Numerical simulation schemes for time-dependent crack growth in hard brittle rock. Acta Geotechnica (2014) DOI 10.1007/s11440-014-0337-9.
[5] Kemeny, J. Time-dependent drift degradation due to the progressive failure of rock bridges along discontinuities. International Journal of Rock Mechanics & Mining Sciences (1995) 42(1), 35-46.
[6] Lee, J.S. Time-dependent crack growth in brittle rocks and field applications to geologic hazards. PhD dissertation (2007), The University of Arizona.
[7] Park, N. Discrete element modeling of rock fracture behavior: fracture toughenss and time-dependent fracture growth. PhD dissertation (2006), The University of Texas at Austin.
[8] Potyondy, D.O. Simulation stress corrosion with a bonded-particle model for rock. International Journal of Rock Mechanics & Mining Sciences (2007) 44, 677-691.
[9] Freiman, S.W. Effect of chemical environments on slow crack growth in glasses and ceramics. J Geophys Res (1984) 89(B6):4072–6.
[10] Atkinson, B.K. Subcritical crack growth in geological materials, J. Geophys. Res (1984) 89, 4077–4114.
[11] Rinne, M. Fracture mechanics and subcritical crack growth approach to model time-dependent failure in brittle rock. PhD dissertation (2008), Helsinki University of Technology.
[12] Hillig, W.B. and Charles R.J. In High-Strength Materials. Edited by V.F.Zackey. John Wiley & Sons, Inc., New York, (1965) pp.682-705.
[13] Wiederhorn, S.M. and Bolz, L.H. Stress Corrosion and Static Fatigue of Glass. J. Am. Cer. Soc. (1970) 53, 544-548.
[14] Wiederhorn, S.M. Fuller, E.R. Jr. and Thomson, R. Micromechanisms of Crack Growth

in Ceramics and Glasses in Corrosive Environments, Metal Science (1980) August-September, pp. 450-458.
[15] Amitrano, D. and Helmstetter, A. Brittle creep, damage and time-to-failure in rocks. Journal of Geophysical Research B: Solid Earth 111 (2006) (B11201 DOI:10.1029/2005JB004252).
[16] Bass, D.J. Elasticity of minerals, glasses and melts, in Mineral Physics and Crystallography, Ref. Shelf Ser., vol. 2, edited by T. J. Ahrens, pp. 45– 63, AGU, Washington, D. C (1995).
[17] Chen, S. Yue, Z.Q. and Tham, L.G. Digital image-based numerical modeling method for prediction of inhomogeneous rock failure. International Journal of Rock Mechanics & Mining Sciences (2004), 41(2004), 939-957.
[18] Yu, Q. Zheng, C. Yang, T. Tang, S. Wang, P. and Tang, C. Meso-structure characterization based on coupled thermal-mechanical model for rock failure process and applications. Chinese Journal of Rock Mechanics and Engineering (2012), Vol.31 No.1, pp. 42-51 (in Chinese).
[19] Potyondy, D.O. and Cundall, P.A. A bonded-particle model for rock. International Journal of Rock Mechanics & Mining Science (2004) 41, 1329-1364.
[20] Schmidtke, R.H. and Lajtai, E.Z. The Long-Term Strength of Lac du Bonnet Granite. Int J Rock Mech Min Sci & Geomech Abstr (1985) 22(6):461-465.